Fuzzy grey predictor compensated time-varying variable structure controller for solar inverters

En-Chih Chang[a], Ziang Xu[a], Zhiyi Su[b] and Rong-Ching Wu[a,*]

[a]*Department of Electrical Engineering, I-Shou University, Dashu District, Kaohsiung City, Taiwan, R.O.C.*
[b]*School of Control Science and Engineering of Shandong University, Jinan, P.R.C.*

Abstract. In this paper, a fuzzy grey predictor (GP) compensated time-varying variable structure controller (TVVSC) is developed and applied to solar inverters. TVVSC can shorten the reaching phase and ensure the sliding mode occurrence from an arbitrary initial state. However, while loading is a severe nonlinear condition, the TVVSC may suffer from chattering and steady-state error problems, thus deteriorating solar inverter performance. A GP is thus devoted to alleviate the chattering when the system uncertainty bounds are overestimated, and to reduce the steady-state error when the system uncertainty bounds are underestimated. However, the GP with a fixed forecasting value causes long rise time or large overshoot of the system response. Thus, fuzzy logic (FL) is applied to obtain flexible forecasting values to improve the system performance. With the proposed controller, the robustness of the solar inverter system can be enhanced, and a high-quality solar inverter sinusoidal output voltage with low voltage harmonics and fast dynamic response can be obtained, even under nonlinear loading. The theoretical analysis, design procedure, computer simulations, and digital signal processing (DSP)-based experimental implementation for solar inverters are presented to verify the efficacy of the proposed controller.

Keywords: Grey predictor (GP), time-varying variable structure controller (TVVSC), fuzzy logic (FL), solar inverter, voltage harmonics

1. Introduction

In recent years, solar inverters have gained increasing attention, and been broadly used in energy conversion systems [4]. In solar energy systems, the overall performance is dependent upon the static inverter-filter arrangement, which is used to convert a DC voltage into a sinusoidal AC output. The requirements for a high-performance solar inverter must supply a high-quality AC output voltage with low total harmonic distortion (THD), zero steady-state error and a fast dynamic response; these can be obtained by employing feedback control techniques. The linear proportional Integral (PI) controller is typically used. However, the classic PI controlled system can not ensure fast and stable output voltage response [7, 9]. Various control techniques have been proposed, such as wavelet transform technique, deadbeat control, and repetitive control, etc. However, these control techniques are difficult to implement and complex in computation [3, 10, 13]. For robust control systems, the variable structure control (VSC) can be adopted because the VSC is insensitive to system

*Corresponding author. Rong-Ching Wu, Department of Electrical Engineering, I-Shou University, No.1, Sec. 1, Syuecheng Rd., Dashu District, Kaohsiung City 84001, Taiwan, R.O.C. Tel.: +886 7 6577711/Ext: 6642; Fax: +886 7 6577205; E-mail: rcwu@isu.edu.tw.

uncertainties, and provides a fast dynamic response. The controller of the solar inverters is also very popularly designed with VSC; however, the design of the classic VSC with fixed sliding surface is employed, and the sliding mode is attained when the system state reaches and maintains on the intersection of the sliding surface [1, 14]. Thus, the trajectories are sensitive to uncertainties before the sliding mode occurs. To improve such problems, the concept of the TVVSC is introduced. The TVVSC is first chosen to pass arbitrary initial conditions and subsequently moved towards a predetermined sliding surface by means of rotating and/or shifting. By employing the time-varying sliding surface, the system sensitivity to uncertainties is reduced by shortening the reaching phase [8, 12]. However, once a highly nonlinear loading is applied, the TVVSC controlled system is subject to chattering and steady-state error, thus resulting in serious voltage harmonics in the solar inverter output, even deteriorating the solar inverter performance. The grey predictor (GP) has been proposed by Deng, and many applications in a variety of fields have been developed. The grey model is built based on first-order differential equations, and utilizes mathematical approximation to transfer a continuous form into a discrete form. Such a transformation will confront some unconquerable problems, such as limited sampling frequency, sample/hold effects and discretization errors. Use of a difference equation replaces the differential equation to build a grey model that provides a reasonable and exact approach [5, 11]. This paper employs a mathematically simple and computationally efficient GP to alleviate the chattering and steady-state error when the system uncertainties are overestimated or underestimated. Though GP requires several output data to achieve a grey model and to forecast a future value without complex calculation, the GP uses a fixed forecasting value and leads to long rise time or large overshoot of the system response. Fuzzy set theory was introduced in 1965 and has received extensive applications. Fuzzy logic (FL) is thus used to tune the GP flexible forecasting value so as to maintain both a short rise time and a small overshoot of solar inverters system response [2, 6]. By combining FL, GP, and TVVSC, the proposed controller will yield a closed-loop solar inverter with low THD, fast dynamic response, elimination of chatter, and steady-state error reduction under various types of loads. Simulation and experimental results are demonstrated to verify the performance of the proposed controller.

2. Solar inverter control design

A representative single-phase solar inverter is shown in Fig. 1, with a DC power supply V_{dc}, resistance load R, PWM full-bridge inverter and L-C filter. The proposed controller is used to design a 1KW 60 Hz solar inverter.

The $L-C$ filter and R are considered to be a plant system, and the dynamics with state variables are expressed as:

$$\dot{x}_{p2} = -a_{p1}x_{p1} - a_{p2}x_{p2} + b_p u_p + d \qquad (1)$$

where $x_m = [x_{p1}\ x_{p2}] = [v_c\ \dot{v}_c]$, $a_{p1} = \frac{1}{LC}$, $a_{p2} = \frac{1}{RC}$, $b_p = \frac{K_{PWM}}{LC}$, K_{PWM} is the proportional gain of the inverter, u_p is the plant input, and d is the uncertainty.

The model system is given by the sinusoidal function with 60 Hz.

$$\dot{x}_{m2} = -a_{m1}x_{m1} - a_{m2}x_{m2} + b_m u_m \qquad (2)$$

where, $x_m = [x_{m1}\ x_{m2}] = [v_{ref}\ \dot{v}_{ref}]$, $a_{m1} = \omega_0^2 = (2\pi \cdot 60)^2$, $a_{m2} = 0$, $b_m = 1$, and u_m is the reference input.

By defining $e_1 = x_{m1} - x_{p1}$, subtracting Equation (1) from Equation (2), the error differential equation yields:

$$\dot{e}_1 = e_2 = \dot{x}_{m1} - \dot{x}_{p1} = x_{m2} - x_{p2} \qquad (3)$$

$$\dot{e}_2 = -a_{m1}e_1 - a_{m2}e_2 + (a_{p1} - a_{m1})x_{p1}$$

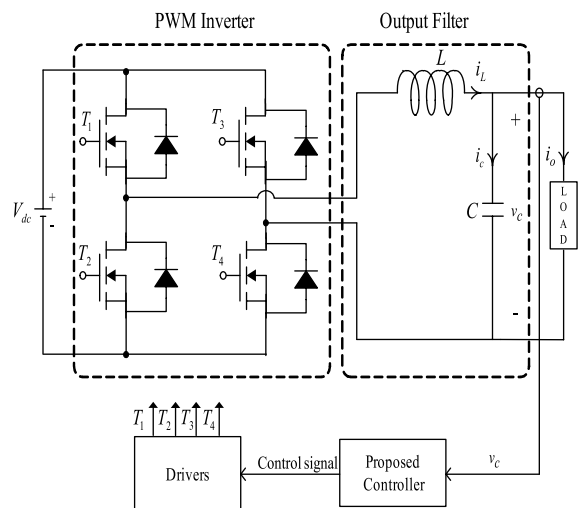$$+ (a_{p2} - a_{m2})x_{p2} + b_m u_m - b_p u_p - d \quad (4)$$

Fig. 1. Block diagram of solar inverter.

Then, the time-varying sliding surface is selected as:

$$\sigma = c_1(t)e_1 + e_2 - \alpha(t) \qquad (5)$$

where $c_1(t) = At + B$; $\alpha(t) = Ct + D$; and A, B, C, D are constants.

Taking the derivative of σ yields:

$$\dot{\sigma} = Ae_1 + c_1(t)e_2 - a_{m1}e_1 - a_{m2}e_2 + (a_{p1} - a_{m1})x_{p1}$$

$$+ (a_{p2} - a_{m2})x_{p2} + b_m u_m - b_p u_p - d - C \quad (6)$$

Define $a_{p_i} = a_{pi}^0 + \Delta a_{pi}$ and $b_p = b_p^0 + \Delta b_p$, and the control function can be expressed as:

$$u_p = u_e + u_s \qquad (7)$$

The equivalent control u_e, which can determine the dynamic of the system on the sliding surface is derived as:

$$Ae_1 + c_1(t)e_2 - a_{m1}e_1 - a_{m2}e_2 + (a_{p1} - a_{m1})x_{p1}$$

$$+ (a_{p2} - a_{m2})x_{p2} + b_m u_m - b_p u_p = 0 \qquad (8)$$

Substituting $u_p = u_e$ into Equation (8) yields:

$$u_e = [Ae_1 + c_1(t)e_2 - a_{m1}e_1 - a_{m2}e_2$$
$$+ (a_{p1}^0 - a_{m1})x_{p1}$$
$$+ (a_{p2}^0 - a_{m2})x_{p2} + b_m u_m - C] \Big/ b_p^0 \qquad (9)$$

When in sliding action:

$$e_2 = -c_1(t)e_1 - \alpha(t) \qquad (10)$$

Substituting Equation (10) into Equation (9) yields:

$$u_e = \frac{[Ae_1 + c_1^2(t)e_1 + \alpha(t)c_1(t) - a_{m1}e_1}{+ c_1(t)a_{m2}e_1 + \alpha(t)a_{m2} + (a_{p1}^0 - a_{m1})x_{p1}} \Big/ b_p^0$$
$$+ (a_{p2}^0 - a_{m2})x_{p2} + b_m u_m - C]$$
$$\qquad (11)$$

The system performance can be ensured despite the existence of the uncertain system dynamics. The sliding control u_s is designed as follows:

$$u_s = K_1 e_1 + K_2 e_2 + K_n \qquad (12)$$

Inserting Equation (12) in $\sigma\dot{\sigma} < 0$, sufficient stability conditions K_1, K_2 and K_n will be obtained.

Notice that if a highly nonlinear loading is connected to solar inverter output, the chattering and steady-state error will occur. Thus, we employ the GP with GM(2,1) model to eliminate the chattering and steady-state error. The GP modeling steps are described below.

Step 1. Gather the original sample data sequence

$$x^{(0)} = \left\{ x^{(0)}(k), \ k = 1, \ 2, \ ..., \ n \right\} \qquad (13)$$

Step 2. Mapping generating operation (MGO).

The data sequence of the system may be positive or negative. The MGO maps the negative data to the relative positive data.

$$x_{new}^{(0)} = \left\{ x^{(0)}(k) + Bias, \ k = 1, \ 2, \ ..., \ n \right\} \quad (14)$$

where *bias* is constant.

Step 3. Take accumulated generating operation (AGO) for $x_{new}^{(0)}$

$$x_{new}^{(1)}(k) = \sum_{i=1}^{k} x_{new}^{(0)}(i), \ k = 1, \ 2, \ ..., \ n \qquad (15)$$

Step 4. Build the GM(2,1) model.

The linear difference equation grey prediction model is established as:

$$x_{new}^{(1)}(k+2) + M x_{new}^{(1)}(k+1) + N x_{new}^{(1)}(k) = 0 \quad (16)$$

where M and N are the coefficients of the difference equation grey prediction model that must estimate their values.

The, Equation (16) is rewritten as the following matrix:

$$\left[-x_{new}^{(1)}(k+1) \ -x_{new}^{(1)}(k) \right] \begin{bmatrix} M \\ N \end{bmatrix} = \left[x_{new}^{(1)}(k+2) \right]$$
$$\qquad (17)$$

Let $k = 1, 2, ..., n-2$ and suppose $Y = \begin{bmatrix} x_{new}^{(1)}(3) \\ x_{new}^{(1)}(4) \\ \vdots \\ x_{new}^{(1)}(n) \end{bmatrix}$,

$$B = \begin{bmatrix} -x_{new}^{(1)}(2) & -x_{new}^{(1)}(1) \\ -x_{new}^{(1)}(3) & -x_{new}^{(1)}(2) \\ \vdots & \vdots \\ -x_{new}^{(1)}(n-1) & -x_{new}^{(1)}(n-2) \end{bmatrix},$$

and $\Theta = \begin{bmatrix} M \\ N \end{bmatrix}$, then the estimated parameters M and N can be solved by the least square estimation method as follows:

$$\Theta = [M, \ N]^T = (B^T B)^{-1} B^T Y \qquad (18)$$

Let $x_{new}^{(1)}(k) = \xi^k$, $x_{new}^{(1)}(k+1) = \xi^{k+1}$, and $x_{new}^{(1)}(k+2) = \xi^{k+2}$; the following equation is obtained:

$$\xi^{k+2} + M\xi^{k+1} + N\xi^k = \xi^k(\xi^2 + M\xi + N) = 0 \quad (19)$$

The roots to satisfy Equation (19) are given as:

$$\begin{cases} \xi_1 = \frac{-M+\sqrt{M^2-4N}}{2} \\ \xi_2 = \frac{-M-\sqrt{M^2-4N}}{2} \end{cases} \quad (20)$$

If $\xi_1 \neq \xi_2$, the solution of the prediction model of the second-order difference equation can be expressed as:

$$\hat{x}_{new}^{(1)}(k) = C_1\xi_1^k + C_2\xi_2^k \quad (21)$$

where "$\wedge$" represents the predicted value, and C_1 and C_2 are constants.

If $\xi_1 = \xi_2$, the solution of the prediction model of the second-order difference equation can be expressed as:

$$\hat{x}_{new}^{(1)}(k) = C_1\xi_1^k + C_2k\xi_1^k \quad (22)$$

If ξ_1 and ξ_2 are complex conjugate, the solution of the prediction model of the second-order difference equation can be expressed as:

$$\hat{x}_{new}^{(1)}(k) = C_1\upsilon^k \sin\phi k + C_2\upsilon^k \cos\phi k \quad (23)$$

Step 5. Take inverse accumulated generating operation (IAGO).

$$\hat{x}_{new}^{(0)}(k) = \hat{x}_{new}^{(1)}(k) - \hat{x}_{new}^{(1)}(k-1) \quad (24)$$

Step 6. Inverse mapping generating operation (IMGO).

Applying IMGO to $\hat{x}_{new}^{(0)}$, the predicted value of the original data sequence $\hat{x}^{(0)}$ is obtained as:

$$\hat{x}^{(0)}(k+1) = \hat{x}_{new}^{(1)}(k+1) - \hat{x}_{new}^{(1)}(k) - Bias \quad (25)$$

Then, the control law of Equation (7) is restated as:

$$u_p(k) = u_e(k) + u_s(k) + u_g(k) \quad (26)$$

where the grey prediction control u_g assists in alleviating chatter and steady-state error.

$$u_g(k) = \begin{cases} 0 & , |\hat{\sigma}(k)| \leq \varepsilon \\ K\hat{\sigma}(k)\text{sgn}(\sigma(k)\hat{\sigma}(k)) & , |\hat{\sigma}(k)| \geq \varepsilon \end{cases} \quad (27)$$

where K is constant, $\hat{\sigma}(k)$ represents the predicted value of $\sigma(k)$, and ε indicates the system boundary. Note that the control law in Equation (7) implies the signum function (sgn($\cdot$)) and requires infinite switching frequency in the theory, to maintain the system states on the sliding surface. However, an infinite switching frequency cannot be realized when the control law is implemented on

a DSP. Thus, using a saturation function $sat(\cdot)$ instead of sgn($\cdot$) provides:

$$sat(\hat{\sigma}(k), \varepsilon) = \begin{cases} \text{sgn}(\sigma(k)) & if |\hat{\sigma}(k)| > \varepsilon \\ \hat{\sigma}(k)/\varepsilon & if |\hat{\sigma}(k)| \leq \varepsilon \end{cases} \quad (28)$$

It is worth noting that the above-mentioned GP uses a fixed forecasting value, and may cause long rise time or large overshoot of the system response. To solve such a problem, FL is introduced to finely tune the GP forecasting value, thus enhancing the system robustness. The operation of fuzzy tuning GP forecasting value is illustrated as follows. Let the predicted error and the change of the predicted error at the kth-step ahead be $\hat{e}_1(k+1)$ and $\Delta\hat{e}_1(k+1)$, respectively. Define $\hat{e}_1$ and $\Delta\hat{e}_1$ as the input of the fuzzy logic, where the $\hat{e}_1$ and $\Delta\hat{e}_1$ are the fuzzy variables of the GP value $\hat{e}_1(k+1)$ and $\Delta\hat{e}_1(k+1)$, respectively. The output of the fuzzy logic (U_{FL}) is the fuzzy variable indicating the forecasting value. The universes of discourse of $\hat{e}_1$, $\Delta\hat{e}_1$ and U_{FL} are partitioned into the following fuzzy sets: NB (Negative Big); NM (Negative Medium); NS (Negative Small); Z (Zero); PB (Positive Big); PM (Positive Medium); PS (Positive Small); VS (Very Small); SM (Small); MD (Medium); LG (Large); VL (Very Large); HU (Huge); and VH (Very Huge); Thus, the FL of a two-input single-output fuzzy model with 49 rules can be obtained as follows:

R^1: If $\hat{e}_1$ is NB and $\Delta\hat{e}_1$ is NB then U_{FL} is VH.
R^2: If $\hat{e}_1$ is NM and $\Delta\hat{e}_1$ is NB then U_{FL} is HU.
$$\vdots$$
R^{49}: If $\hat{e}_1$ is PB and $\Delta\hat{e}_1$ is PB then U_{FL} is VH.

3. Simulation and experimental results

The system parameters of the solar inverter are given as follows: DC-bus voltage, $V_{dc} = 200$ V; switching frequency, $f_s = 15$ kHz; output voltage and frequency, $v_c = 110$ V$_{rms}$, $f = 60$ Hz; rated resistive load, $R = 12\ \Omega$; filter inductor, $L = 1.5$ mH; filter capacitor, $C = 15\ \mu$F. Figure 2(a) depicts the simulated transient response with the load changing from no load to full load at $t = 0.0208$ s for the proposed controller. The transient response of the proposed controller is very fast, taking only a few sampling intervals to reach steady-state. On the contrary, the simulated waveforms shown in Fig. 2(b) with classic VSC indicates a significant voltage sag. A simulated performance testing, shown in Fig. 2(c) is achieved by applying a nonlinear load consisting of a diode bridge, a capacitor (100 μF) and a

(a) (50V/div; 20A/div).

(b) (50V/div; 20A/div).

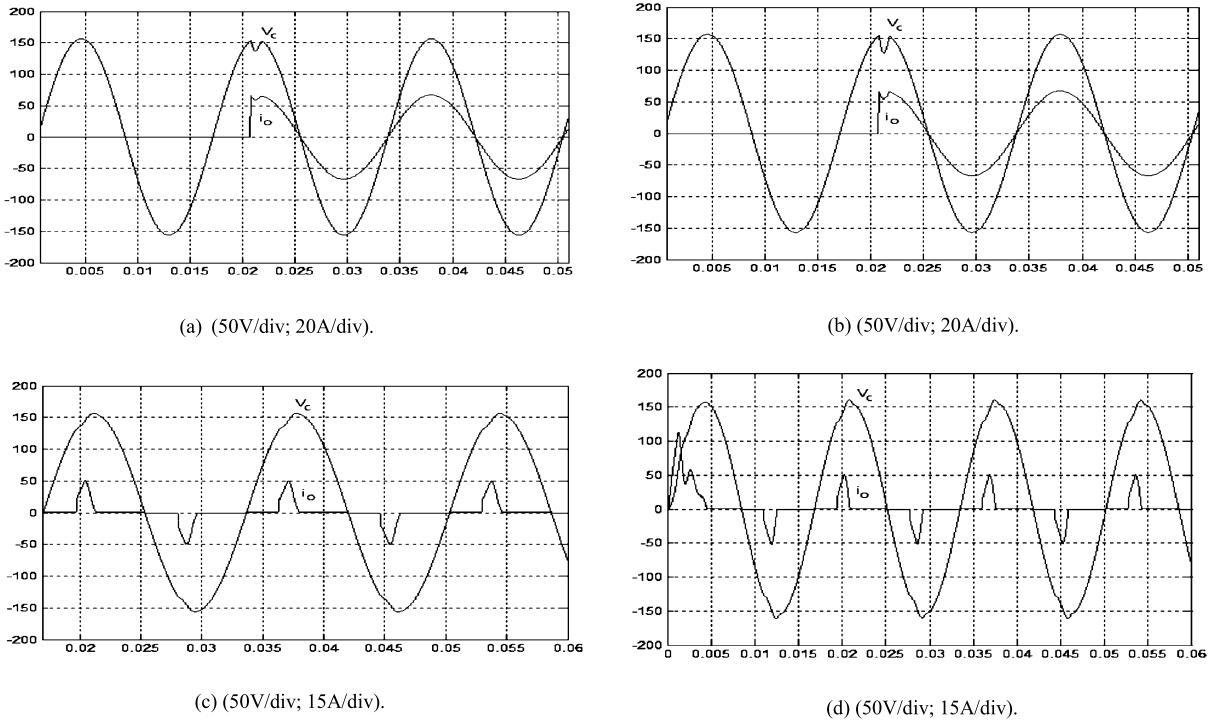(c) (50V/div; 15A/div).

(d) (50V/div; 15A/div).

Fig. 2. Depicts the simulation results of output voltage and load current under (a) step change in load with the proposed controller; (b) step change in load with classic VSC; (c) rectifier load with proposed controller; (d) rectifier load with classic VSC.

(a) (100V/div; 20A/div; 5ms/div).

(b) (100V/div; 20A/div; 5ms/div).

(c) (100V/div; 20A/div; 5ms/div).
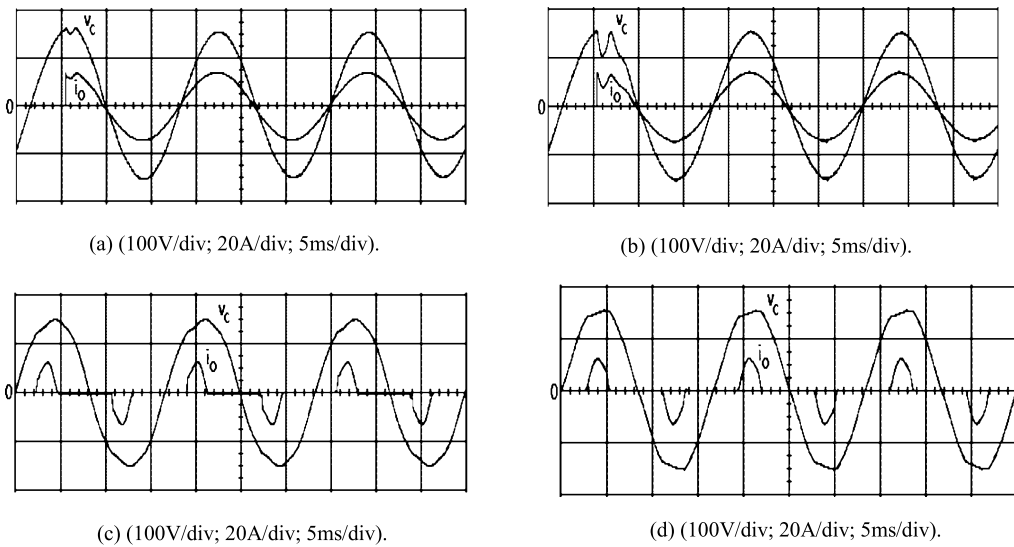

(d) (100V/div; 20A/div; 5ms/div).

Fig. 3. Experimental waveforms under (a) step change in load with the proposed controller; (b) step change in load with classic VSC; (c) rectifier load with proposed controller; (d) rectifier load with classic VSC.

resistive load (60 Ω). The simulated %THD computed in the output voltage is 1.13%; The AC voltage is still satisfactory, and good behavior of the inverter is also obtained in this critical condition. However, under the

same rectifier loading obtained using the classic VSC, shown in Fig. 2(d), exhibits a high simulated %THD output voltage (%THD of output voltage is equal to 8.01%). Figure 3(a) displays the experimental output

voltage and the load current with the proposed controller under a load step change from open circuit to $R = 12\Omega$. A rapid recovery of the steady-state response can be obtained. However, the experimental waveform with the classic VSC, shown in Fig. 3(b), demonstrates poor voltage compensation, especially at the firing angle. Additionally, the majority of sensitive loads are rectifier loads. When the diodes are conducting, the inverter is exposed to a large filter capacitor, and when the diodes are not conducting, the inverter is practically in no load condition. Therefore, the controller must correctly regulate output voltage with minimum distortion. Figure 3(c) shows the experimental output voltage and the load current with the proposed controller when the inverter is loaded with a full-wave rectifier followed by a $100\,\mu\text{F}$ capacitor in parallel with a 60Ω resistor; the experimental %THD is close to 1.17%, which indicates good inverter performance. On the contrary, Fig. 3(d) with the classic VSC under the same test condition exhibits a high experimental voltage %THD of 7.42%.

4. Conclusions

A fuzzy GP-compensated TVVSC has been proposed to improve the tracking behaviors of solar inverters. The TVVSC can shorten the reaching phase, thus enhancing the robustness of the system. However, with the application of a highly nonlinear loading, chattering and steady-state error occur. For high tracking accuracy, the GP is used to eliminate the chattering and steady-state error, which are produced by TVVSC. Additionally, FL is added to GP to tune the forecasting value, thus enhancing the system robustness and speed. Simulation and experimental results indicate that low THD, fast transient response, the elimination of the chattering, and the reduction of the steady-state error are obtained by the proposed controlled solar inverter under both steady-state loading and transient loading.

Acknowledgments

References

[1] A. Abrishamifar, A.A. Ahmad and M. Mohamadian, Fixed switching frequency sliding mode control for single-phase unipolar inverters, *IEEE Trans on Power Electronics* **27**(5) (2012), 2507–2514.

[2] A. Syropoulos *Theory of Fuzzy Computation* Springer-Verlag, New York, 2014.

[3] D. Chen, J.M. Zhang and Z.M. Qian, An improved repetitive control scheme for grid-connected inverter with frequency-adaptive capability, *IEEE Trans. on Industrial Electronics* **60**(2) (2013), 814–823.

[4] F.L. Luo and H. Ye *Power electronics: Advanced conversion technologies*, CRC Press 2010.

[5] G.D. Li, S. Masuda, D. Yamaguchi, M. Nagai and C.H. Wang, An improved grey dynamic GM(2,1) model, *International Journal of Computer Mathematics* **87**(7) (2010), 1617–1629.

[6] H. Abu-Rub, A. Iqbal, S. MoinAhmed, F.Z. Peng, Y. Li and B.M. Ge, Quasi-Z-source inverter-based photovoltaic generation system with maximum power tracking control using ANFIS, *IEEE Trans on Sustainable Energy* **4**(1) (2013), 11–20.

[7] I. Rasoanarivo, S. Brechet, A. Battiston and B. Nahid-Mobarakeh, Behavioral analysis of a boost converter with high performance source filter and a fractional-order PID controller, *Proc IEEE Int Conf Industry Applications Society Annual Meeting* (2012), 1–6.

[8] J. Geng, Y.Z. Sheng and X.D. Liu, Second-order time-varying sliding mode control for reentry vehicle, *International Journal of Intelligent Computing and Cybernetics* **6**(3) (2013), 272–295.

[9] R.S. Rebeiro and M.N. Uddin, Performance analysis of an FLC-based online adaptation of both hysteresis and PI controllers for IPMSM drive, *IEEE Trans on Industry Applications* **48**(1) (2012), 12–19.

[10] S.A. Saleh and M.A. Rahman, Experimental performances of the single-phase wavelet-modulated inverter, *IEEE Trans on Power Electronics* **26**(9) (2011), 2650–2661.

[11] S. Liu and Y. Lin *Advances in Grey Systems Research*, Springer-Verlag, Heidelberg, Berlin, 2010.

[12] S. Tokat, I. Eksin and M. Guzelkaya, Linear time-varying sliding surface design based on co-ordinate transformation for high-order systems, *Transactions of the Institute of Measurement and Control* **31**(1) (2009), 51–70.

[13] X.G. Zhang, W.J. Zhang, J.M. Chen and D.G. Xu, Deadbeat control strategy of circulating currents in parallel connection system of three-phase PWM converter, *IEEE Trans on Energy Conversion* **29**(2) (2014), 406–417.

[14] X. Hao, X. Yang, T. Liu, L. Huang and W.J. Chen, A sliding-mode controller with multiresonant sliding surface for single-phase grid-connected VSI with an LCL filter, *IEEE Trans on Power Electronics* **28**(5) (2013), 2259–2268.